IOP Conf. Series: Materials Science and Engineering **416** (2018) 012058 doi:10.1088/1757-899X/416/1/012058

Comparison of the Corrosion Behaviour of Differently Deposited PVD TiN/TiO_2 Coatings on Electron Beam Modified Ti5Al4V Alloy

M P Nikolova[1,*], E Yankov[1], T Hikov[2], D Dechev[2], N Ivanov[2], S Parshorov[3], V Zaharieva[1] and P Petrov[2]

[1]University of Ruse "A. Kanchev", Dept. of Material Science and Technology, 8 Studentska Str., Bulgaria
[2]Bulgarian Academy of Sciences, Institute of Electronics, 72 Tzarigradsko Chausse Blvd, Sofia, Bulgaria
[3]Bulgarian Academy of Sciences, Institute of Metal Science, Equipment and Technologies with Hydro- and Aerodynamics Centre "Akad. A. Balevski", 67 Shipchenski Prohod Blvd, Sofia, Bulgaria

[*]Corresponding author: mpnikolova@uni-ruse.bg

Abstract. In the particular study, the micropatterning of the Ti5Al4V alloy in as-received, solution treated and solution and precipitated condition was done using electron beam surface modification (EBSM) by scanning electron beam. The nanostructured TiN/TiO_2 films were deposited over the EBSM Ti5Al4V substrates using dc magnetron sputtering and cathodic arc and glow-discharge methods. The electrochemical potentiodynamic tests were performed in Ringer saline at 37±0.05 °C and a pH of 5.7 in order to determine the corrosion resistance behavior of the coated and uncoated EBSM substrates as compared with the bare as-received, solution treated and solution and precipitated samples. The presented results gave an idea of the corrosion behavior of the examined implant systems in aggressive environment and external conditions close to the body right.

1. Introduction

The constituting materials for hard endogenous prosthesis should ensure the mechanical stability of the bone-implant system. The former should also lower the friction forces and enhance the anchoring thus permitting fast bone to implant fixation. The exclusively used α+β titanium alloys as supporting materials suffer from toxicity, low fatigue and wear at sliding resistance [1]. When using a functional coating that lowers the friction and stimulates osseointegration, some drawbacks of the titanium alloys could be overcome. Hard and thin TiN coatings generally present high tribological properties while the TiO_2 is among the mostly used biocompatible materials showing good cell adhesion [2]. The combination of nanoscale coating deposited on microscale roughened surface (known as the hierarchical modification) is thought to be favorable for the cell adhesion and formation of components of the extracellular matrix [3]. The electron beam surface modification (EBSM) gives the opportunity of obtaining reproducible isotropic textures with regular surface pattern without any surface contamination of the titanium alloy [4]. Simultaneously, the nanotexture of a PVD coating and the micropatterning of the surface could significantly change the corrosion resistance of the titanium alloys. The TiN and TiO_2 films are generally thought to be chemically inert. As the PVD deposition process usually generates many small defects such as pinholes which size and quantity are highly dependent on the preparation

conditions, the corrosion behavior of a coated implant system will depend on the extent of these defects. Yilbas B S et al. [5] reported that an adequate defect-free and dense structure of a TiN coating could improve considerably the corrosion resistance of a material. Other authors [6] stated that the TiO_2 coatings improve the corrosion resistance by acting as protective layer on steel surface. According to Perillo P M [7], the charge carriers' density of a TiO_2 film on TiN one is significantly higher than that of TiO_2 formed on pure Ti. The titanium alloys themselves are able to form amorphous titanium dioxide that is stable over a wide range of potentials and pH [8]. In case of α+β titanium alloy, the β-phase preferentially dissolves during the long-term exposure in aggressive corrosion media [9]. Hence, treatments that change the phase composition of the alloy such as quenching, precipitation as well as electron-beam modification should affect the corrosion properties of the material. In this scenario, the intention of the particular work is to compare the electrochemical behavior of Ti alloy before and after the heat-treatment process and EBSM with those coated by magnetron sputtering and cathodic arc and glow-discharge methods.

2. Experimental procedures

The chemical compositions of the bare Ti substrate and the target material used for the experiment, determined by JEOL JXCA-733 Microprobe scanning electron microscope (SEM) equipped with wavelength dispersive spectrometers (WDS), were shown in Table 1. Samples with dimensions 14×14×4 mm were cut using the electro-erosion cutting method. The as-received (AR) samples were single solution treated (ST) for 30 min at 920 °C and water quenched. Half of the specimens were precipitated (P) for 4 hours at 500 °C and air cooled. All treatments were carried out in ≤ 1 Pa vacuum. The surfaces of the samples were grounded and polished before the EBSM. To study the effect of the surface treatment, the EBSM was applied to AR, ST, and ST and precipitated (ST+P) samples.

Table 1. Chemical composition (wt. %) of the substrate material.

Element	Al	V	Fe	Mn	Co	Cr	Mo	Pd	Nb	Hf	Ti
Substrate	5.21	4.40	0.14	0.11	0.06	-	0.17	0.15	0.36	0.04	Bal.

The EBSM was carried out by electron beam installation Leybold Heraeus (EWS 300/15–60). The following technological parameters were applied electron beam current – I = 20 mA, accelerated voltage – U = 52 kV, speed of the samples motion – v = 0.5 cm/s, electron beam frequency – f = 1 kHz, electron beam diameter - d = 0.5 mm and linear manner of scanning. Afterward, all samples were ultrasonically washed with absolute ethanol, acetone, isopropanol, rinsed with distilled water for 5 min and dried.

The TiN/TiO_2 coating was applied by two different methods - reactive magnetron sputtering (MS) and cathodic arc and glow-discharge method using Ti targets with purity of 99.8%. The deposition of the magnetron TiN layer took a place in the Ar-N_2 atmosphere, as the working pressure was 1.2×10^{-1} Pa, during the deposition process, the substrate had been heated to 350° C. The TiO_2 film was realized in the pure O_2 environment, the working pressure was 7×10^{-2} Pa, as the substrate temperature was decreased down to 180° C. The thickness of each coating (i.e. TiN and TiO_2, respectively) was about 1 μm assessed by the resonant frequency of quartz plate (Intermetalix IL800) coated within the same process conditions. In order to minimize the residual stresses and the oxidation, the samples with deposited coating were retrieved from the vacuum chamber after the achievement of room temperature.

For the cathodic arc deposition of the TiN, a sidewall positioned evaporating system in a cubic vacuum chamber with water-cooled walls was used. The samples were hanged near the center of a clockwise-rotating with a frequency of 0.5 Hz turntable. To ensure the coating stress relaxation and necessary adhesion, a very thin pure layer from the target (at 2.5×10^{-1} Pa in Ar atmosphere for 5 min., bias 600 V, 110 A arc current) was applied. The TiN film was made in a pure N_2 atmosphere at 340 °C substrate temperature for a time of 60 min., 110 A arc current, bias 250 V and 7.5×10^{-1} Pa pressure in the working chamber. The TiO_2 film was made by glow plasma discharge using the uppermost located sputtering pure Ti system in the same chamber. A bias voltage of 1340 V (720 mA current) in a pure O_2 atmosphere at a pressure of 6×10^{0} Pa were applied for a deposition time of 240 min. Both layers' thickness (TiN ~ 2.7 μm, TiO_2 ~ 0.8 μm) was attained by calotest measurements.

The X-ray phase identification was performed with URD-6 diffractometer, applying Bragg-Brentano geometry and Cu-Kα radiation and working at 30 kV and 20 mA. The diffraction angle range scanned was 2θ = 20-100° with a step size of 0.05° and counting time of 2.5 s/step. The light optical microscopy was performed on the top surface and cross-section of the samples after Kroll's reagent etching using a Nikon microscope equipped with a 14-megapixel digital camera.

The electrochemical study was held in experimental set-up comprised the electrochemical cell with a platinum counter electrode and a saturated Ag/AgCl reference electrode. Both electrodes together with the working one with 0.2 cm^2 exposed area were immersed in 80 ml naturally aerated Ringer solution (RS) for infusion (8,60 g/L NaCl, 0.30 g/L KCl, and 0.33 g/L $CaCl_2.2H_2O$) at 37±0.05 °C to simulate the in-body environment. The pH of the solution equal to 5.70±0.02 at 37° C was measured using a portable HI 8424 pH meter (Hanna instruments) that was fitted with a pH glass electrode (HI 1230B). The open circuit potentials (OPC) were measured at 0.25 s intervals as a function of the immersion time for 1000 s. After the OPC, potentiodynamic polarization curves were recorded by sweeping the potential starting at a cathodic potential about 250 mV below the E_{ss} (steady state potential) up to +2000 mV vs. Ag/AgCl at a scan rate of 1 $mV.s^{-1}$ using a potentiostat 263A (EG&G Princeton Applied Research) coupled to a PC by a controller. All OPC and potentiodynamic measurements were repeated at least twice in order to ensure repeatability of the experimental results. The corrosion parameters E_{corr} (corrosion potential) and I_{corr} (corrosion current density) were obtained from the polarization curves by Tafel extrapolation method. I_{pass} (passivation current density) was attained by measuring the current density values around the middle of the passivation region of the polarization plot. The polarization resistance (R_p) was determined from the Stern-Geary equation.

3. Results and discussions

The micrographs of the AR, ST, and ST+P Ti54 together with the corresponding topographic images of the re-melted grains obtained on the surface after the EBSM of the material are shown in Figure 1.

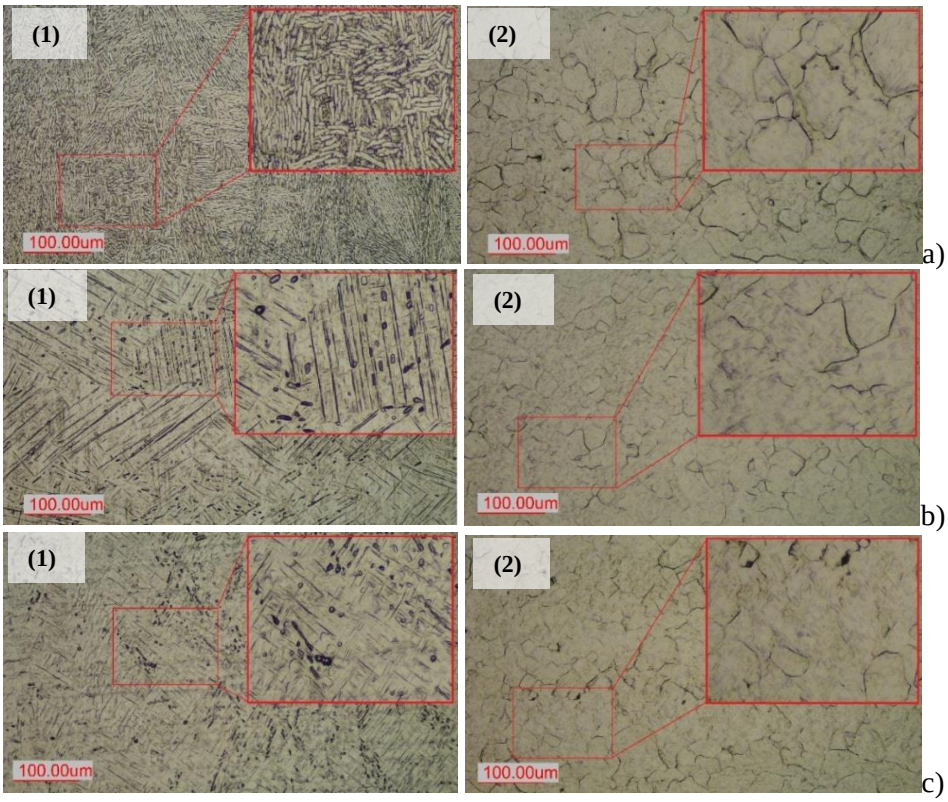

Figure 1. Micrographs of the AS (a), ST (b) and ST+P (c) samples before (1) and after the EBSM (2). The images marked with "1" are cross-sections of the AR and heat-treated samples, while the micrographs "2" represent topographic views after the EBSM.

The XRD spectra of all coated and non-coated materials are displayed in Figure 2. The coarse α+β lamellar structure of the AR material (Figure 1 a-1) after the ST from α+β range contained predominantly gross α'-martensite (Figure 1 b-1) formed due to the diffusionless β→α' transformation and some undissolved globular α-phases in between them. As the primary α phase and α'-martensite had the same inter-planar spacing of the HCP crystal structure, their distinction by XRD analysis is difficult. The precipitation after the ST led to element partitioning effect. As known, α'-martensite decomposes to the ordered Ti_3Al phase that was not detected by optical microscopy observations (Figure 1 c-1) but the shift of the ST+P α-reflections towards higher angle, as opposed to the ST sample (Figure 2), confirmed the decreased inter-planer spacing of the phase. The EBSM changed the XRD patterns of the material and the top surface morphology where well-defined boundaries of the smaller-sized grains were distinguished (Figure 1-(2)). Within these grains, fine martensite laths together with small pits at the grains' boundaries were present. The MS coatings deposited on the surface of the EBSM samples indicated only small anatase peaks of the surface oxide layer as well as strong (111) and (200) nitride reflections (Figure 2). In contrast, the glow-discharge deposited oxide on the arc-PVD nitride showed two distinctive TiO_2 phases – anatase and rutile, dominated by the rutile phase. The arc deposited nitride sub-layer mainly consisted of (200) and (220) textured crystal lattices.

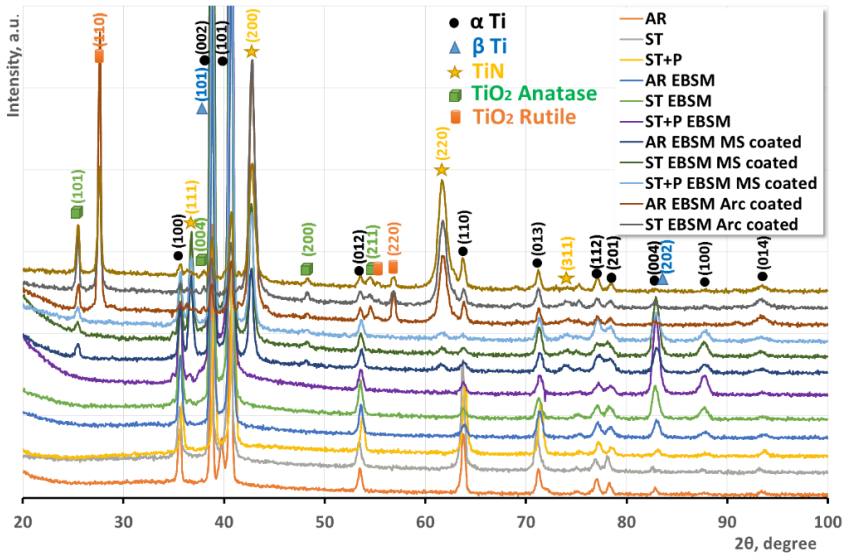

Figure 2. XRD patterns of the AS, heat treated, EBSM and coated samples by arc and MS methods.

The steady state potentials (E_{ss}) in time of the AR, heat-treated and EBSM samples (Figure 3 a) displayed a positive shift of the E_{ss} after precipitation of the alloy (from -475 mV to -320 mV) suggesting an increase in the corrosion resistance of the alloy in ST+P condition. Simultaneously, the ST+P EBSM curve was located at the top with the ST EBSM curve just below it. Hence, the re-melted and homogenized surface structures obtained after EBSM showed better corrosion resistance especially when the alloy was in ST and ST+P conditions probably because of the thicker passive layer. The E_{ss} of the coated samples (Figure 3 b) outperformed the potentials of the non-coated samples with the exception of the EBSM ST and ST+P specimens. The spontaneous passivation process of the AR EBSM Arc coated sample was interrupted by fluctuations probably because of short terms activation and passivation changes. In general, all OCPs of the coated samples showed close values varying between -16 and -92 mV vs. Ag/AgCl. However, the E_{ss} shift to more positive or negative values is not a certain criterion of low or high corrosion rate.

The coated and uncoated alloy displayed similar passive properties with low current density values suggesting low corrosion ratio. The corrosion potential of the ST (E_{corr} = -0.447 V) sample was slightly higher than that of the AR (E_{corr} = -0.486 V) while that of the ST+P was better (E_{corr} = -0.286 V) than that of the ST one (Figure 4 a). These findings could be attributed to the heterogeneous α+β composition

of the AR alloy [4] resulting in lower corrosion resistance of the material because of galvanic cell formation [10]. The results suggest that both α and Ti_3Al phases that had similar crystallographic structures decreased the crystallographic mismatch of the phases existing within the lamellar structure of the AR and outperformed the corrosion resistance of the unstable acicular structure of the ST sample. Excluding the small peak in the current density of the ST+P sample at ~1.75V, the passivation behavior of all three samples represented lack of potential breakdowns in the anodic part of the potentiodynamic curve indicating high pitting corrosion resistance during the electrochemical measurements.

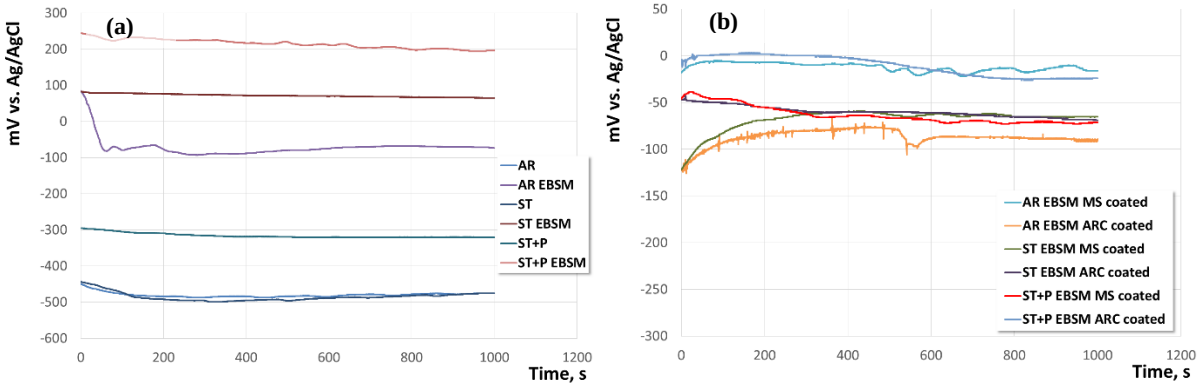

Figure 3. Open circuit potential *E = f(t)* in RS (pH 5.7) and 37±0.05°C temperature of the: a) AR, heat treated and EBSM samples; c) TiN/TiO_2 coated samples

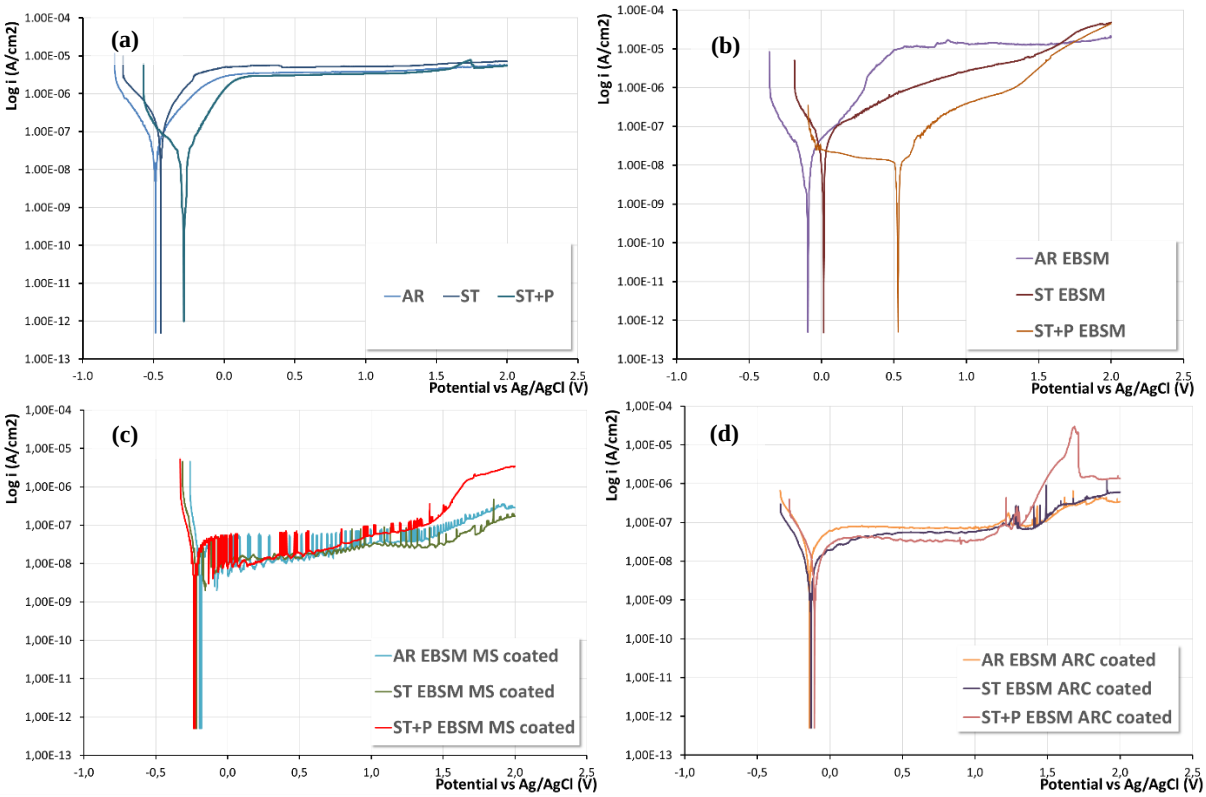

Figure 4. Potentiodynamic polarization curves *log/i/ = f(E)* of the samples in a RS (pH 5.7) at 37±0.05 °C: a) AR and heat-treated alloy; b) EBSM alloy in AR, ST, and ST+P condition; c) MS coated EBSM alloy; d) Arc coated EBSM alloy.

All corrosion potentials of the EBSM samples indicated a tendency of more positive shift (Figure 4 b). Therefore, the evenly distributed alloying elements in all phases form uniformly distributed oxide clusters. The current densities of the ST and ST+P EBSM samples increased with the potential. In

contrast, after breaking down of the initial film of the AR EBSM specimen, another stable state was formed but at higher passive current density (~13.3 μA/cm^2) as opposed to the AR (~3.9 μA/cm^2), ST (~5.3 μA/cm^2) and ST+P (~3.4 μA/cm^2). For the heat-treated and EBSM samples with smaller grains detected on the re-melted surface [4], the positive slope in the anodic current density indicated that the protective film was becoming less protective and more defective [7]. The intensification of the interaction of chloride ions with the surface could be associated with the increase in roughness of the EBSM samples while the lack of flat passive area could be due to the surface grains' morphology.

The ceramic structures of the MS and Arc deposited coatings (Figure 4 c and d) increased the R_p, charge transport and improve the electrochemical barrier properties of the surface. In contrast to the previous samples, the cathodic polarization curves of the coated samples did not show active dissolution areas. The oscillation in the current density of the MS coated samples in the passive region (Figure 4 c) could suggest the anatase broke down by micro-sized pitting nucleations and re-passivations (metastable pits formation [8]). These localized breakdowns were observed throughout the whole anodic parts of the curves. Hence, the electrochemical behavior of the MS deposited coating conforms to the morphology of the surface porosity. However, the passive corrosion currents of all MS coated samples had extremely low values indicating that a very protective film was formed.

The preliminarily formed anatase- and rutile-containing layers deposited on the surface of the Arc-obtained TiN (Figure 4 d) decreased the accessibility of the solution to the TiN that contains many diffusion paths around the droplets. The current density in the cathodic domain was almost one order of magnitude lower than the MS coated samples indicating decreased reduction reactions. The passive current density varied among ~0.076 μA.cm^{-2} and ~0.036 μA.cm^{-2} for the AR and St+P EBSM and Arc coated samples, respectively, indicating a higher corrosion resistance compared to the non-coated alloy. At potentials above ~1.2 V vs. Ag/AgCl, the current density increased forming peaks that some authors [11, 12] associated this with the formation of Ti compounds or structural changes inside the film [13]. In this area, localized breakdowns of the passive oxide by the anions were also detected in the potentiodynamic curve. In contrast to the MS coated samples, the microscopic breakdown events occurred after the passivation region (~ 0 - 1.25 V). The rapid increase of the current indicated the transition into transpassive state until stable pits were formed. At potentials higher than 1.5 – 1.8 V second passive region was observed at higher passivation current density. It is obvious that the oxide layers inhibit a process of anodic dissolution.

Table 2. Values of the electrochemical parameters: E_{corr} - corrosion potential; I_{corr} - corrosion current density; I_{pass} - passivation current density; R_p - polarization resistance; E_{ss} – steady state potential

Ti54 material	**E_{corr} (mV)** vs. Ag/AgCl	**I_{corr} (μAcm^{-2})**	**I_{pass} (μAcm^{-2})**	**R_p (MΩ)**	**E_{ss}, (mV)** vs. Ag/AgCl
AR	-486	0.04	3.86	0.20	-475
ST	-447	0.22	5.25	0.22	-475
ST+P	-286	0.017	3.33	0.24	-320
AR+EBSM	-104	0.02	13.30	-	-73
ST+EBSM	19	0.04	2.77*	-	64
ST+P+EBSM	552	0.015	0.39*	-	194
AR+EBSM MS coated	-190	0.034	0.034	1.8	-16
ST+EBSM MS coated	-219	0.030	0.029	2.7	-65
ST+P EBSM MS coated	-230	0.042	0.052	6.7	-71
AR+EBSM Arc coated	-140	0.084	0.072	6.6	-89
ST+EBSM Arc coated	-135	0.014	0.053	24.7	-68
ST+P EBSM Arc coated	-101	0.014	0.036	11.9	-25

* I_{pass} for ST+EBM and ST+P+EBM was determined at 1V.

The increase of E_{corr} seen in the coated and especially in the EBSM samples indicated that the material was less prone to corrosion (Table 2). With regard to the corrosion current density that is proportional to the corrosion rate, the ST+P, ST+P EBSM, and ST+P EBSM Arc coated samples showed slightly lower values compared to the ST sample, although of the same order of magnitude (Table 2). A tendency of decreasing the corrosion current density after heat treatment of the EBSM alloy was seen for the Arc coated materials while the corrosion current densities of the MS coated specimens displayed very close

values. On increasing the potential, most samples formed protective anodic oxide films but the passive current of the coated specimens showed significantly lower values than the AR, heat treated and AR+EBSM samples. The R_p values which represents the resistance to corrosion in the particular solution indicated the highest values for the Arc coated samples and the lowest for the AR specimen. This implies that the coated samples have a very good corrosion resistance and low rate of ion release from the surface.

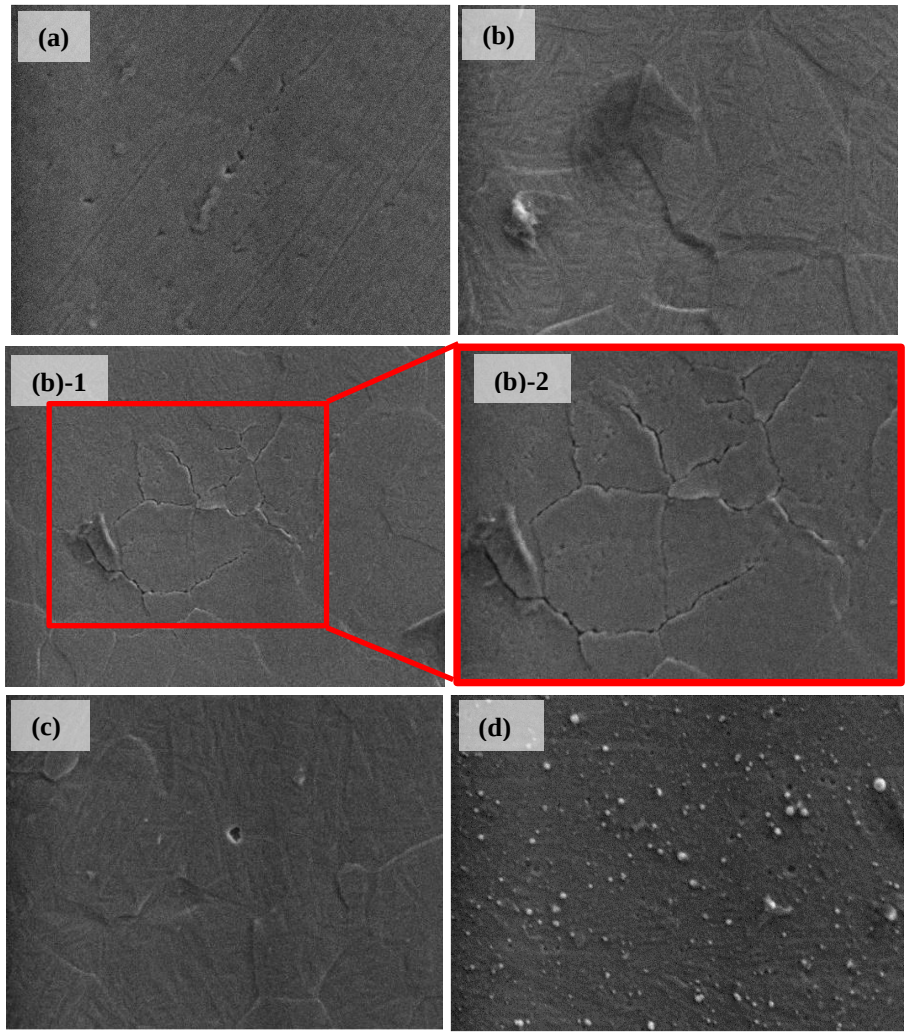

Figure 5. SEM micrographs (SE mode) of the surface of the samples (1000×) after the corrosion tests: (a) ST; (b, b-1 (600×) and b-2) different areas of the AR+EBSM surface; (c) AR+EBSM MS coated; (d) AR+EBSM Arc coated sample.

Figure 5 showing the SEM micrographs after the electrochemical tests, indicated the presence of localized defect areas. The detrimental aggressive attack of the Cl^- ions on the materials' surfaces caused the formation of lots of small pits over the entire surface of the ST sample. As seen in Figure 5 b, corrosion process triggered surface changes spread over larger areas of the AR and EBSM sample, predominantly located around the grain boundaries. Rarely, grain boundary pits surrounding and separating certain grains and some located inter-granularly (Figure 5b-1) were also noticed. Few pits could be observed on the surface of the MS coated sample (Figure 5 c) while those on the AR EBSM Arc coated specimen appeared to be smaller but with the higher amount (Figure 5 d), which explained its slightly higher I_{corr} values.

4. Conclusions

As the passivity of the titanium alloy occurs by the formation of a stable oxide film, the presence of chlorides in the solution enhances the stability and passivation and thus the innate resistance of the alloy in AR and heat-treated (ST and ST+P) condition. The ST+P treatment and EBSM strongly influence the OPC values of the Ti54 alloy in RS but the treatment with high energy fluxes makes the surface more susceptible to pitting corrosion especially for the finer grained ST and EBSM samples that show lack of passive area in the particular conditions. The improved values of the electrochemical parameters of the EBSM alloy could be attributed to the higher passivity of the homogenized electron-beam re-melted surface. However, these layers could not be perfect isolating barriers to ions release but they could act as an intermediate barrier that reduces the corrosion rate. This is so because as seen from the electrochemical parameters, the corrosion resistance is much dependent on the passivation ability of the substrate and the micro-defects in the coating. The RS stimulates pits formation on the coated samples but at different time periods – metastable pits in the whole anodic part of the MS coated samples and stable pits after 1.25 V anodic potential for the ARC and glow discharged oxidized samples. Further examination of the exact mechanism of the growing metastable pits in physiological solution should be performed. The results from the particular study show that the deposited coatings could be allocated to the noble metal surface treatments that could be used for facilitating biocorrosion prevention. Both complex TiN/TiO_2 coatings offer improved corrosion resistance and capability to withstand the aggressive conditions of the RS at 37 °C.

5. References

[1] Manam N S, Harun W S W, Shri D N A, Ghani S A C, Kurniawan T, Ismail M H and Ibrahim M H I 2017 *J. Alloys Compd* **701** 698-715
[2] Kommireddy D S, Patel A A, Shutava T G, Mills D K and Lvov Y M 2005 *J. Nanosci. Nanotechnol.* **5** (7) 1081-1087
[3] Misra S K and Boccaccini A R 2007 Biodegradable and bioactive polymer/ceramic composite scaffolds, *Tissue Engineering Using Ceramics and Polymers*, 72-92, ISBN: 9781845691769
[4] Nikolova M P, Yankov E, Petrov P, Valkov S, Ormanova M, Zaharieva V, Tonev D and Andreeva A 2017 Electron Beam Surface Modification Of Ti5Al4V Alloy For Biomedical Applications *Conf. Proc. Metal 2017*, pp 1555-59
[5] Yilbas B S, Sahin A Z, £oban A 1995 Wear and corrosion properties of PVD TiN coated Ti-6Al-4V materials, Transactions on Engineering Sciences **8**, ISSN 1743-3533
[6] Burnat B, Dercz G, Blaszczyk T 2014 J Mater Sci: Mater Med **25** 623–63
[7] Perillo P M 2015 Corrosion Behaviour of Titanium Nitride Coating on Titanium and Zircaloy-4, American Journal of Materials Science and Application **3** (2) 18-25
[8] Heakal F E-T, Shehata O S and Tantawy N S 2014 *Int. J. Electrochem. Sci*. **9** 1986-2004
[9] Atapour M., Pilchak A L, Frankel G S, Williams J C 2011 Corrosion behavior of β titanium alloys for biomedical applications, Mater Sci & Eng C **31** 885–891
[10] Song H-J, Kim M-K, Jung G-C, Vang M-S and Park Y-J 2007 *Surf & Coat Techn* **201** 8738–8745
[11] Assis S L, Wolynec S and Costa I 2006 Corrosion characterization of titanium alloys by electrochemical techniques *Electrochim Acta* **51** 1815–1819
[12] Pohrelyuk I M, Fedirko V M, Tkachuk O V and Proskurnyak R V 2014 Corrosion Resistance of Titanium Alloys with Oxynitride Coatings in Concentrated Inorganic Acids *Mater. Sci.* **50** (2) 269-276
[13] Zhu M, Wang R, Chen C, Zhang H and Zhang G 2017 Electrochemical study on the corrosion behavior of Ti_3SiC_2 in 3.5% NaCl solution, *RSC Advances* 7, 12534–12540

Acknowledgments

The present research was supported by a contract with National Science Fund (NSF) of Bulgaria, (D№ 07/3 (2016), Gradient functional nanocoatings produced by vacuum technologies for biomedical applications).